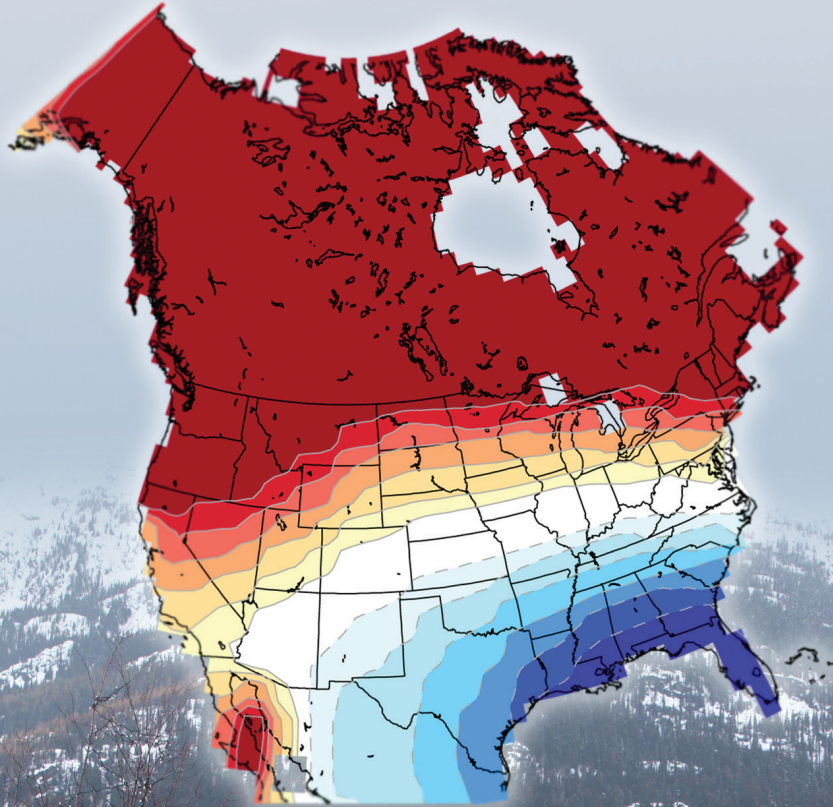# STATE OF THE CLIMATE

IN 2010

J. Blunden, D. S. Arndt, and M. O. Baringer, Eds.

Associate Eds. K. M. Willett, A. J. Dolman, B. D. Hall, P. W. Thorne, J. M. Levy, H. J. Diamond, J. Richter-Menge, M. Jeffries, R. L. Fogt, L. A. Vincent, and J. M. Renwick

5. THE ARCTIC—J. Richter-Menge and M. Jeffries, Eds.

a. Overview—J. Richter-Menge and M. Jeffries

This chapter describes observations of continuing change in the Arctic environmental system. It is organized into five broad sections: atmosphere, ocean, sea ice cover, land, and Greenland. The land section includes vegetation, permafrost, river discharge, terrestrial snow, and glaciers outside Greenland.

The year 2010 marks the end of the warmest decade on record in the Arctic since instrumental records began in 1900. The distribution of near-surface air temperature anomalies over the entire Arctic region continued to show a factor of two (or more) amplification relative to lower latitudes. Changes throughout the Arctic system exemplify this broad pattern of persistent warming and its integrated consequences. For instance:

- Events in Greenland in summer 2010 epitomize the high rate and magnitude of environmental change that is occurring in the Arctic. Unprecedented high surface and upper air temperature were the result of a persistent atmospheric circulation pattern that favored northward advection of warm air along the west side of Greenland in particular. The warm air from the south was responsible for the longest period and largest area of ice sheet melt since at least 1978, and the highest melt rate since at least 1958.

- West of Greenland, high summer air temperatures and a longer melt season also occurred in the Canadian Arctic, where the rate of mass loss from small glaciers and ice caps continued to increase. At the circum-Arctic scale, with the exception of Scandinavia, a combination of low winter (2009/10) snow accumulation and high spring air temperatures resulted in a record minimum spring snow cover duration.

- Eight of the ten smallest summer sea ice minima have occurred in the last decade, and the September 2010 Arctic sea ice extent was the third lowest of the past 30 years. After a record minimum summer sea ice cover in 2007, the upper Arctic Ocean remains relatively warm and fresh, a condition that is affecting marine biology and geochemistry.

- Observations of circumpolar changes to tundra vegetation indicate continued increases in greening associated with more abundant ice-free coastal waters and higher tundra land surface temperatures. Temperatures in coastal permafrost in northernmost Alaska continue to increase and there is evidence that the warming is propagating inland. Rising air and land temperatures continue to have hydrological consequences, with an earlier and more rapid rise in Eurasian river discharge in 2010.

b. Atmosphere—J. Overland, M. Wang, and J. Walsh

For the last decade, the average annual temperature over Arctic land has been the warmest in the record beginning in 1900 (Fig. 5.1). The annual mean air temperature for 2010 mirrored 2009, with slightly lower temperatures than in recent years. The distribution of 2010 annual average near-surface air temperature anomalies over the entire Arctic region continued to show a factor of two (or more) amplification relative to lower latitudes (Fig. 5.2a). This distribution was dominated by above-normal temperatures in northern Canada, the Baffin Bay region, including the west coast of Greenland, and the Pacific side of the central Arctic.

In general, all of the seasonal composites indicate widespread positive air temperature anomalies throughout most of the Northern Hemisphere relative to the baseline years of 1968–96 (Figs. 5.2b–e). Springtime above-normal temperature anomalies were observed from the Siberian Arctic coastal zone across to northern Baffin Bay and the west coast of Greenland and south into the northeastern U.S. (Fig. 5.2c). This continued the springtime pattern seen in the previous decade. These conditions set the stage for record-setting onset to spring snow melt across much
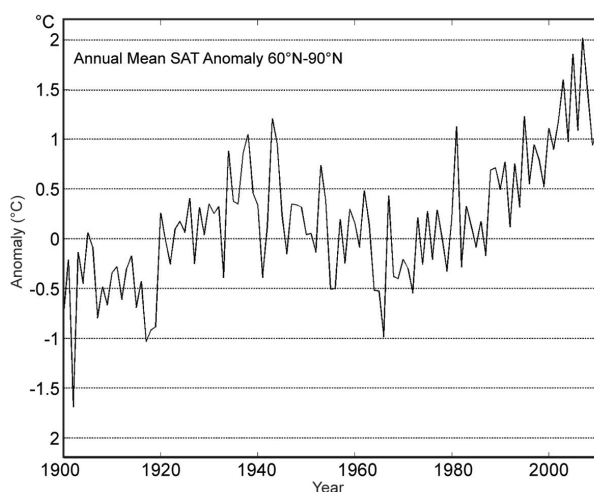

Fig. 5.1. Arctic-wide annual average surface air temperature (SAT, °C) anomalies relative to the 1961–90 mean, based only on land stations north of 60°N. Data are from the CRUTEM 3v dataset, http://www.cru.uea.ac.uk/cru/ data/temperature/.
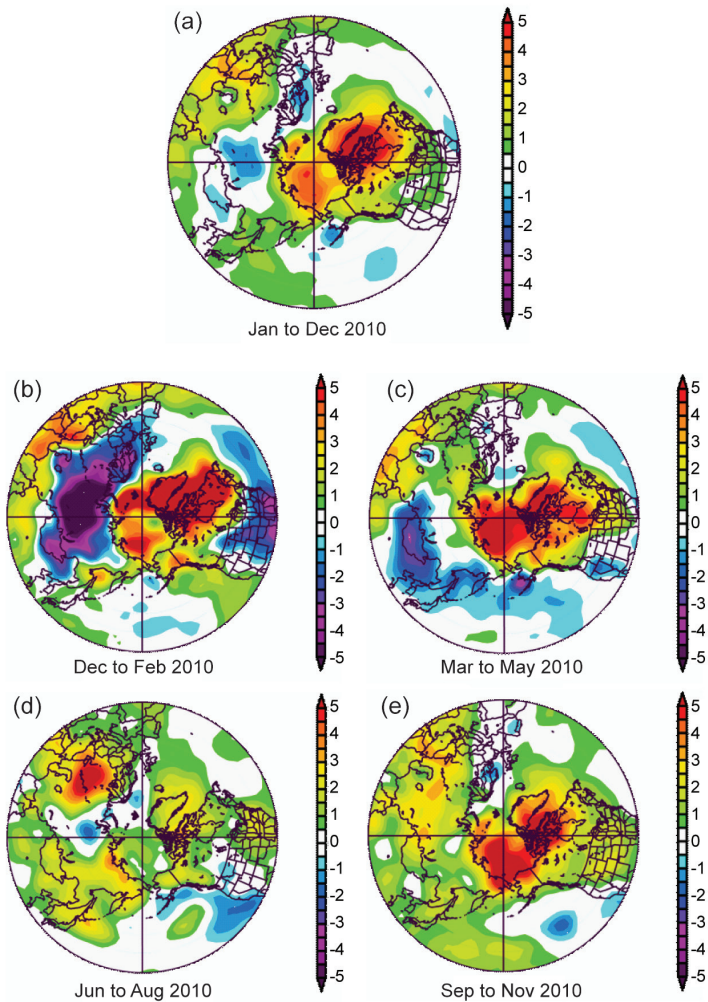
FIG. 5.2. Near-surface (1000 mb) air temperature (°C) anomalies, relative to the 1968–96 mean according to the NCEP/NCAR Reanalysis of the NOAA Earth Systems Research Laboratory (ESRL). (a) January–December 2010; (b) December 2009–February 2010; (c) March–May 2010; (d) June–August 2010; and (e) September–November 2010. These charts were generated online at www.cdc.noaa.gov.

A strong meridional atmospheric circulation pattern in winter facilitated the advection of cold air from the Arctic southward into eastern midlatitude North America and Asia and northern Europe (Figs. 5.3a,b; Seager et al. 2010b). This has been called the Warm Arctic-Cold Continent climate pattern and is associated with a weak polar vortex. In winter, cold air is normally maintained in the Arctic by strong polar vortex winds consistent with a low geopotential height field and strong vorticity over the central Arctic. Two indicators of a weak polar vortex are a negative Arctic Oscillation index (AO) and a negative North Atlantic Oscillation (NAO) index (see Sidebar 1.1). December 2009 through February 2010 had the lowest NAO values in 145 years of historical record. Very negative AO values also occurred in the same period and in December 2010. Negative (cold) temperature anomalies during February and December 2010 over land in Siberia helped to offset its warm anomalies in spring and fall, thus giving lower annual mean values than in other recent years (Fig. 5.1).

Balancing the wintertime events that create a southerly flow of cold air towards the midlatitudes are regions of warm air moving northward during the same months. For example, warm anomalies are observed in December 2010 covering all of Greenland, northeastern Canada, and far eastern Siberia (Fig. 5.3b). The combination of overall warm anomalies in spring, summer, and fall combined with the warm Arctic-cold
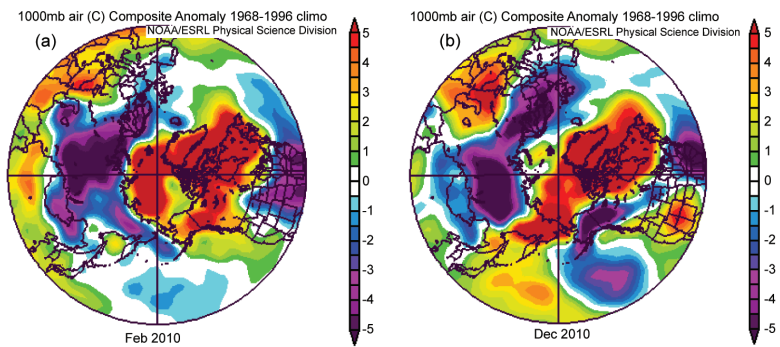
of the Arctic region, contributing to a shorter-than-normal snow season (see section 5e4) and record-setting surface air temperatures along west Greenland (see section 5f). They also reflect the distribution of ice loss observed in arctic glaciers outside of Greenland (see section 5e5). Autumn shows a pattern of temperature anomalies (Fig. 5.2e) that relates to summer sea ice loss north of Alaska and eastern Siberia and from northeastern Canada and Baffin Bay (see section 5d1).

FIG. 5.3. The Warm Arctic-Cold Continent climate pattern for (a) February 2010 and (b) December 2010 illustrated by air temperature (°C) anomalies from the normal 1000 mb air temperature values observed during 1968–96. Data are from the NCEP/NCAR Reanalysis of NOAA ESRL. The charts were generated online at www.cdc.noaa.gov.

continent pattern in winter, gave a large positive temperature anomaly to west Greenland throughout the year. This included summer (June–August, Fig. 5.2d), with a pattern of warm anomalies over the Baffin Bay region and the east Siberian coastal region, similar to but weaker than spring and fall (Figs. 5.2c,e).

c. *Ocean*—A. Proshutinsky, M.-L. Timmermans, I. Ashik, A. Beszczynska-Moeller, E. Carmack, I. Frolov, M. Itoh, T. Kikuchi, R. Krishfield, F. McLaughlin, S. Nishino, B. Rabe, U. Schauer, K. Shimada, V. Sokolov, M. Steele, J. Toole, W. Williams, R. Woodgate, M. Yamamoto-Kawai, and S. Zimmermann

1) WIND-DRIVEN CIRCULATION

In 2010, the annual wind-driven ocean circulation regime was anticyclonic (clockwise) with a well-organized Beaufort Gyre and relatively weak transpolar drift system (Fig. 5.4). The current anticyclonic circulation regime has persisted since 1997, i.e., for 13 years, instead of the typical five to eight year pattern (Proshutinsky and Johnson 1997). It may be that after the anomalous 2007 conditions (a historical minimum of September sea ice extent and maximum upper-ocean warming and freshening) the Arctic climate system bifurcated towards a new state characterized by a more persistent anticyclonic regime and with relatively small changes from year to year.
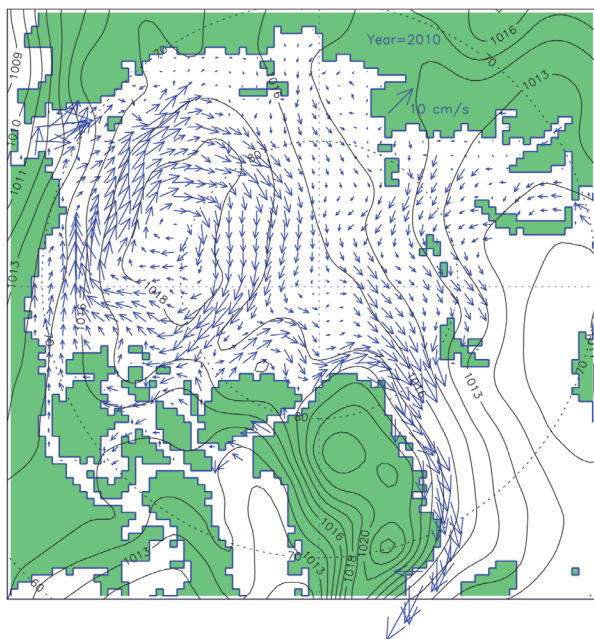

FIG. 5.4. Annual 2010 simulated wind-driven ice motion (arrows) and sea level atmospheric pressure (hPa, black lines). Results are from a 2-D coupled ice-ocean model (Proshutinsky and Johnson 1997, 2011) forced by wind stresses derived from 2010 NCEP/NCAR reanalysis six-hourly sea level pressure fields.

2) OCEAN TEMPERATURE AND SALINITY
(i) Upper ocean

Upper-ocean temperature anomalies in summer 2010 (Fig. 5.5) were comparable to those in 2009 but remained lower than the record set in 2007 (Proshutinsky et al. 2010) Interannual variations in sea surface temperature (SST) anomalies reflect differences in the pace of sea ice retreat, as well as changing advection of warm ocean currents from the south (Steele et al. 2010). In recent years, solar radiation has penetrated more easily into the upper ocean under thinning and retreating ice cover to create high near-surface temperature maxima (Jackson et al. 2010; Yang 2009; Toole et al. 2010; McPhee et al. 2009).

Relative to the 1970s, surface waters in the Arctic Ocean in 2009–10 (Fig. 5.6) were generally saltier in the Eurasian Basin and fresher in the Canadian Basin, with the maximum freshwater anomaly centered in the Beaufort Gyre. The western Canada Basin surface waters were fresher in 2009 and 2010 than in 2007 and 2008, with saltier surface waters in the eastern Canada Basin. The region between Greenland and the North Pole was generally fresher in 2009–10 than in 2007–08, while the upper ocean was saltier in the western Makarov Basin in 2009 and 2010 (Timmermans et al. 2011).

(ii) Beaufort Gyre freshwater and heat content

The Beaufort Gyre (BG) is the largest reservoir of freshwater in the Arctic Ocean. In 2010, the magnitude of BG freshwater content was comparable to 2008 and 2009 conditions; however, the region of freshwater tended to spread out from the 2007–09 center (Fig. 5.7, right panels). During 2003–10, the BG accumulated more than 5000 km^3 of freshwater, a gain of approximately 25% (update to Proshutinsky et al. 2009) relative to climatology of the 1970s. The Beaufort Gyre heat content (Fig. 5.7, left panels) in 2010 increased relative to 2009 by approximately 5%.

Freshwater increases were not limited to the BG. Observations of the upper ocean freshwater content for the entire Arctic Ocean indicate that from 1992–99 to 2006–08 the freshwater content increased by 8400 ± 2000 km^3 (Rabe et al. 2011).

(iii) The Atlantic water layer

Warm water of North Atlantic origin, the Atlantic water layer (AWL), resides between approximately 200 meters and 900 meters and is characterized by temperatures greater than 0°C and salinities greater than 34.5. In 2009–10, AWL maximum temperature anomalies were generally highest on the Eurasian side
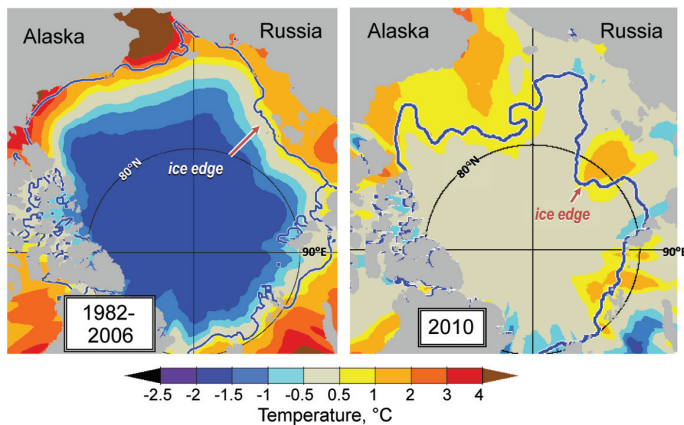
FIG. 5.5. Summer (June–September) SST anomalies in 2010 (right panel) relative to the summer mean during 1982–2006 (left panel). The anomalies are derived from satellite data according to Reynolds et al. (2002). The September mean ice edge (thick blue line) is also shown.
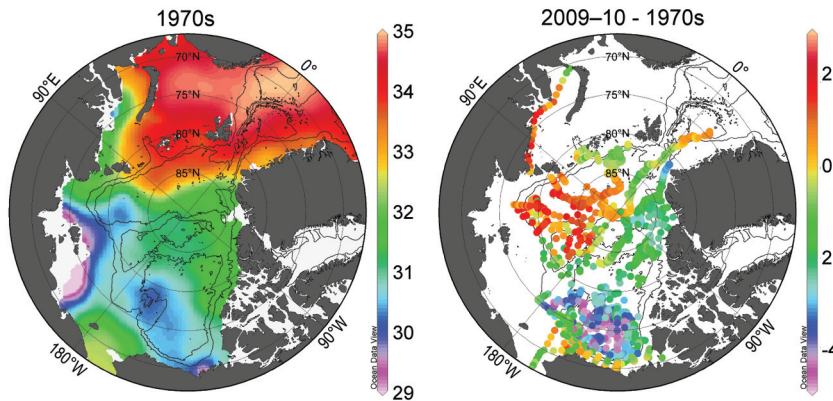

FIG. 5.6. Anomalies of salinity at 20 m depth in 2009–10 (right) relative to 1970s climatology (left). The 500 m and 2500 m isobaths have been plotted using the IBCAO grid.

winter AW temperatures were slightly higher in 2009/10 than the previous year, while in summer 2010 the mean temperature remained close to that observed in summer 2009, with typical substantial seasonal variability.

(iv) The Pacific water layer

The Pacific water layer (PWL) is located in the Canada Basin at depths between approximately 50 meters and 150 meters (Steele et al. 2004) and originates from the Bering Strait inflow. The relatively warm and fresh PWL (S < 33.5) comprises about two-thirds of the Canadian Basin halocline by thickness and about half by freshwater content (e.g., Aagaard and Carmack 1989). In the period 2002–06 the PWL penetrated into the Beaufort Sea from the southern end of the Northwind Ridge, but in 2007–10 it took a different path, spreading northward along the Chukchi Plateau directly from the Herald Canyon (Fig. 5.9, lower panels). These changes in the physical environment cause changes in the biogeochemical environment (see section 5c3).

The characteristics of Pacific waters depend on water properties and transport, and atmospheric conditions in the Bering Strait. Preliminary data suggest that in 2008 and 2009 Pacific waters were slightly cooler than during 2002–07, but warmer than during 1999–2001. The 2009 volume transport (~0.9 Sv) was slightly higher than in 2008, but still less than the 2007 transport (> 1 Sv), which was the highest in the available record (spanning 1991–95 and 1998–2009). The 2009 heat flux was close to the long-term mean, while the freshwater flux in 2009 was somewhat higher than the mean (due in part to the higher-than-average transports), but still less than previous maxima in 2004 and 2007.

3) BIOLOGY AND GEOCHEMISTRY

As described above, the quantity of freshwater stored in the Beaufort Gyre increased substantially in 2007–10 due to both inputs of sea ice melt water (Yamamoto-Kawai et al. 2009) and strong Ekman pumping conditions (updates to Proshutinsky et al.

of the Lomonosov Ridge, with maximum values about 1°C along the boundaries of the Eurasian Basin (Fig. 5.8). Warming was less pronounced in the Canada Basin than in the Eurasian Basin. There was little to no temperature anomaly (< 0.1°C) at the southeast boundary of the Canada Basin or in the basin boundary regions adjacent to Greenland and the Canadian Archipelago. Negative (cooling) temperature anomalies were detected in the vicinity of Nares Strait.

The characteristics of the AWL are regulated by the Atlantic water (AW) properties and transport at the inflow in Fram Strait. After reaching a maximum in 2006, AW temperature in Fram Strait decreased in 2007 and 2008. In 2009, AW temperature and salinity in northern Fram Strait increased, returning in summer 2010 to the long-term mean. The autumn and

2009 and Yang 2009) that increased the depth of the upper halocline in the Canada Basin interior. These two effects combined to deepen the nitracline and the underlying associated chlorophyll maximum (McLaughlin and Carmack 2010). A consequence of the increased stratification is that overall nitrate fluxes are diminished, a condition which limits new production and favors smaller organisms at the base of the food web (Li et al. 2009). Another consequence of halocline deepening is that the nutricline and chlorophyll maxima are further removed from sunlight, and light limitation may play a greater role. The potential response of basin waters to climate forcing scenarios is thus distinct from scenarios on continental shelves which, in contrast, are expected to become more productive because of increased wind exposure and shelf-break upwelling (Yang 2009) that bring Pacific summer waters into the euphotic zone (Carmack and Chapman 2003). Preliminary analysis from 2010 shows a shallower chlorophyll maximum than in 2009, consistent with the slight relaxation of the Beaufort Gyre in 2009.

Over the Chukchi Abyssal Plain, nutrient-rich water typically results in a strong chlorophyll maximum layer (~3 µg L^{-1}; Nishino et al. 2008). With sufficient nutrient availability, sea ice loss (and subsequent increased solar insolation) can enhance biological primary productivity in this region (Nishino et al. 2009). In 2010, however, increased surface freshening, vertical stratification, and nutricline deepening over the Chukchi Abyssal Plain resulted in a decrease of the chlorophyll maximum (< 0.5 µg L^{-1}).

Undersaturation of the surface waters of the Canada Basin with respect to aragonite, a relatively soluble form of calcium

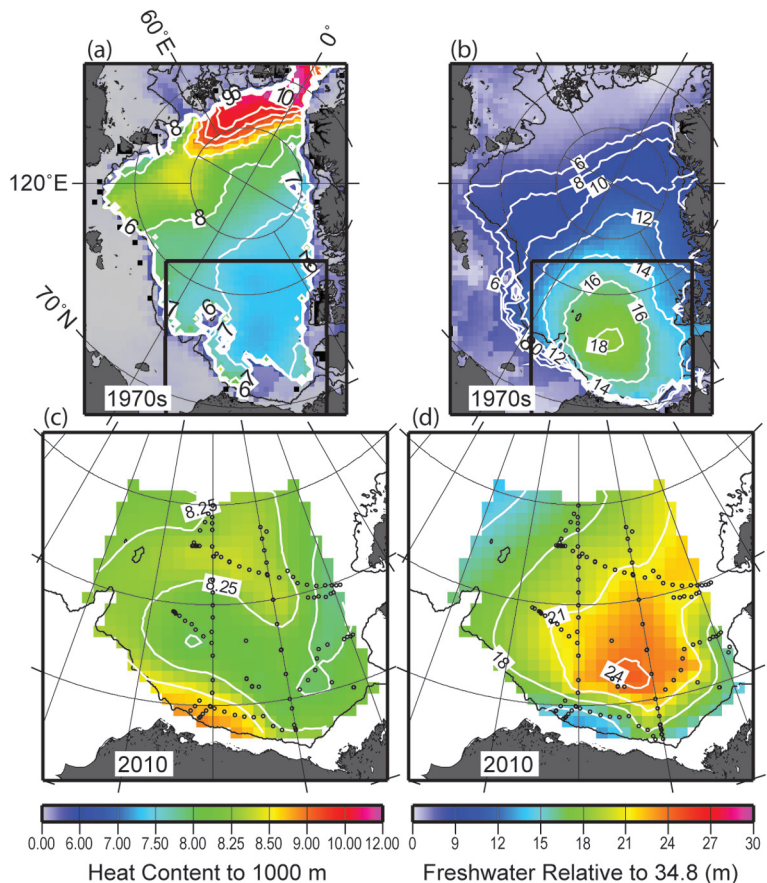FIG. 5.7. Summer heat (× 10^{10} J m^{-2}) and freshwater content to the depth (m) of the 34.8 isohaline. The top row shows (a) heat content and (b) freshwater content in the Arctic Ocean based on 1970s climatology (Timokhov and Tanis 1997, 1998). The bottom panels show (c) heat content and (d) freshwater content in the Beaufort Gyre based on hydrographic surveys (black dots depict hydrographic station locations) in 2010. The Beaufort Gyre region is shown by black boxes in (a) and (b). Heat content is calculated relative to freezing temperature in the upper 1000 m of the water column.
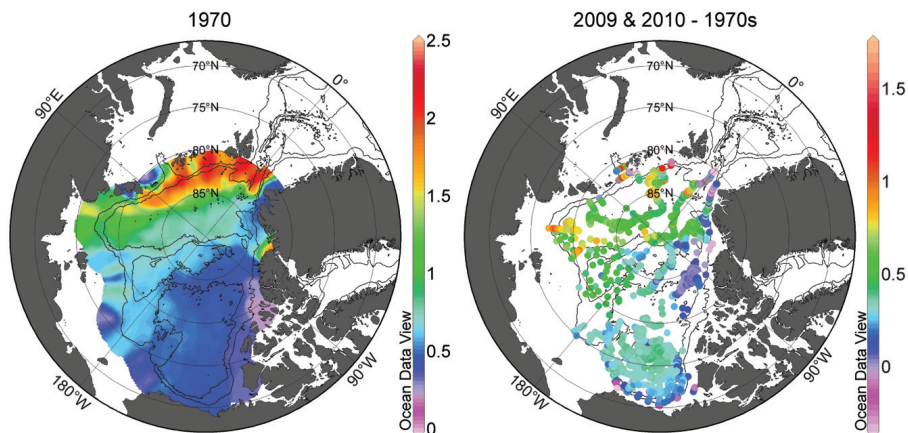

FIG. 5.8. Atlantic warm layer temperature maximum in °C. Left: 1970s climatology. Right: anomalies relative to 1970s climatology. The 500 m and 2500 m isobaths have been plotted using the IBCAO grid.
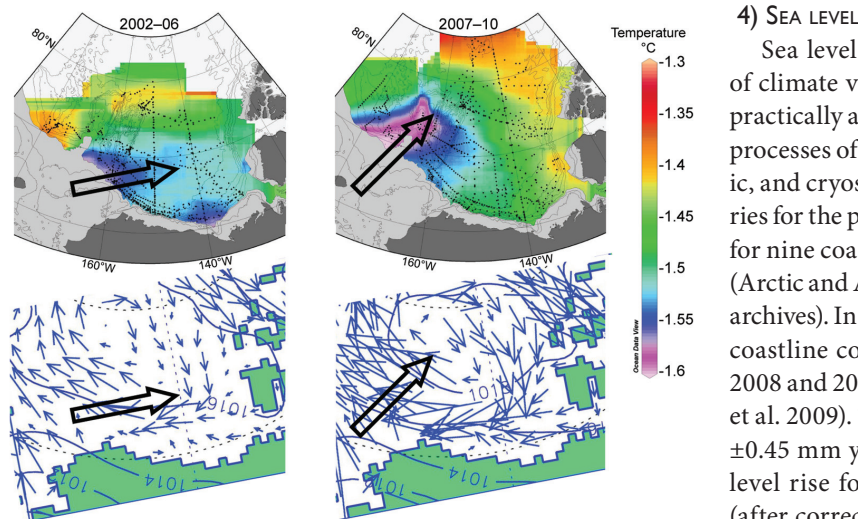
Fig. 5.9. Top panels: potential temperature (°C) in the Canada Basin at the S = 33.1 isohaline. Bottom panels: sea level atmospheric pressure (hPa) and simulated wind-driven component of ice drift. Left and right panels: 2002–06 and 2007–10, respectively. Large arrows show suggested spreading of Pacific winter waters.

carbonate found in plankton and invertebrates, was first observed in 2008 (Yamamoto-Kawai et al. 2009). The areal extent of the surface undersaturation increased in 2009 (results are not yet available for 2010). The reduction in the aragonite saturation state, Ω, is due to a number of factors. Yamamoto-Kawai et al. (2011) estimate that an increase in atmospheric carbon dioxide (CO_2) has lowered surface Ω by ~0.3 in the Canada Basin since the pre-industrial period. Recent melting of sea ice has further lowered mean Ω by 0.4, and of this, half was due to dilution of surface water and half was due to the change in air-sea disequilibrium state. Surface water warming has generally counteracted the mean decrease in Ω by 0.1.

The increased stratification and decrease in upper layer nutrient concentrations have also resulted in an increase in the number of picoplankton and a decrease in nanoplankton (Li et al. 2009). This trend of increasing summer picoplankton abundance in the upper water column of the Canada Basin was recorded in the previous five years. In 2009, there was evidence of a continued increase in picoplankton in late summer and early autumn, but only for the heterotrophic (bacterial) component. In contrast, an apparent departure from this trend for the picophytoplankton in 2009 indicates interannual variability and strong seasonality in the photosynthetic component, which leads to an aliased time series.

4) Sea level

Sea level is a natural integral indicator of climate variability. It reflects changes in practically all dynamic and thermodynamic processes of terrestrial, oceanic, atmospheric, and cryospheric origin. Sea level time series for the period of 1954–2010 are available for nine coastal stations in the Siberian seas (Arctic and Antarctic Research Institute data archives). In 2010, sea level along the Siberian coastline continued to decrease relative to 2008 and 2009 (see Fig. 5.10 in Proshutinsky et al. 2009). This caused a reduction, to 2.49 ±0.45 mm yr^{-1}, in the estimated rate of sea level rise for the nine stations since 1954 (after correction for glacial isostatic adjustment; Proshutinsky et al. 2004).

d. Sea Ice Cover—D. Perovich, W. Meier, J. Maslanik, C. Haas, and J. Richter-Menge

1) Sea ice extent

Sea ice extent is the primary variable for describing the state of the Arctic sea ice cover. Passive microwave satellites have routinely and accurately monitored ice extent since 1979. There are two periods that define the annual cycle and thus are of particular interest: March, at the end of winter, when the ice is at its maximum extent, and September, when it reaches its annual minimum. Ice extent in March 2010 and September 2010 are shown in Fig. 5.10.
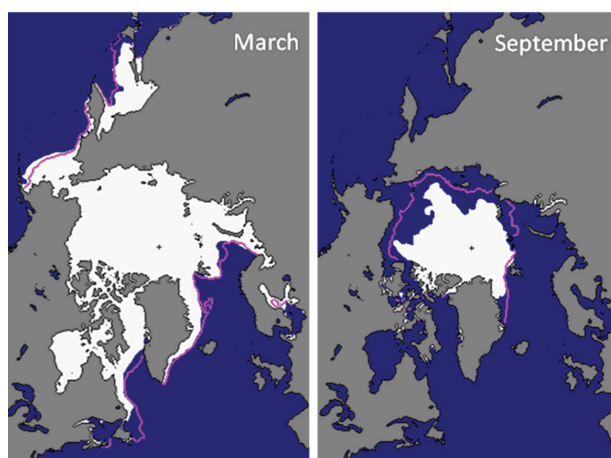

Fig. 5.10. Sea ice extent in March 2010 (left) and September 2010 (right) illustrates the winter maximum and summer minimum extents, respectively. The magenta line indicates the median maximum and median minimum ice extent each month for the period 1979–2000.

On 19 September 2010, ice extent reached its annual minimum, an area of 4.6 million km². This is the third-lowest minimum recorded since 1979, higher only than 2008 and the record minimum in 2007. Overall, the 2010 minimum was 31% (2.1 million km²) lower than the 1979–2000 average. The last four summers have experienced the four lowest minima in the satellite record, and eight of the ten lowest minima have occurred during the last decade. Surface air temperatures through the 2010 summer were higher than normal throughout the Arctic, though less extreme than in 2007 (Stroeve et al. 2008). A strong atmospheric-driven wind surface circulation pattern during June 2010 pushed the ice away from the Alaskan and eastern Siberian coasts. However, the pattern did not persist through the summer as it did in 2007.

The March 2010 ice extent was 15.1 million km², about 4% less than the 1979–2000 average of 15.8 million km². Winter 2010 was characterized by a very strong atmospheric circulation pattern that led to higher-than-normal temperatures (see section 5b). Maximum ice extent occurred on 31 March. This was the latest date for maximum ice extent observed in the 30-year satellite record and was due primarily to late ice growth in the Bering and Barents Seas and the Sea of Okhotsk.

Time series of sea ice extent anomalies in March and September for the period 1979–2009 (Fig. 5.11) show a pronounced decline of -11.6% per decade, with large interannual variability in September summer

FIG. 5.12. Sea ice age in the first week of March, derived by tracking the drift of parcels of ice floes with satellite data, illustrates the substantial loss of old ice in the Arctic Basin in recent years compared to the late 1980s. (a) 1988, (b) 2008, (c) 2009, and (d) 2010. (Figure courtesy of National Snow and Ice Data Center, J. Maslanik and C. Fowler.)

minimum ice extent. The March winter maximum ice extent has also declined, but at a slower rate of -2.7% per decade.

2) Sea ice age

The age of the ice is another key descriptor of the state of the sea ice cover, since older ice tends to be thicker and more resilient than younger ice. Figure 5.12 shows that there has been a substantial loss of old, and thus thick ice in the Arctic Basin in recent years compared to the late 1980s (Kwok 2007; Nghiem et al. 2007; Maslanik et al. 2007). Following the record melt of summer 2007, there was a record-low amount of multiyear ice (ice that has survived at least one summer melt season) in March 2008. There was then a modest increase in multiyear ice in both 2009 and 2010. However, even with this recovery, 2010 had the third lowest March multiyear ice extent since 1980. Most of the two- to three-year old ice remained in the central Arctic during winter 2009/10. A lobe of older ice moved into the Beaufort and Chukchi Seas from the region of old thick ice north of the Canadian Archipelago. Despite being old and presumably relatively thick, Fig. 5.10 indicates this lobe of ice likely did not survive the 2010 summer melt period. Consistent with these observations, data from upward-looking sonars in the Beaufort Gyre (http://
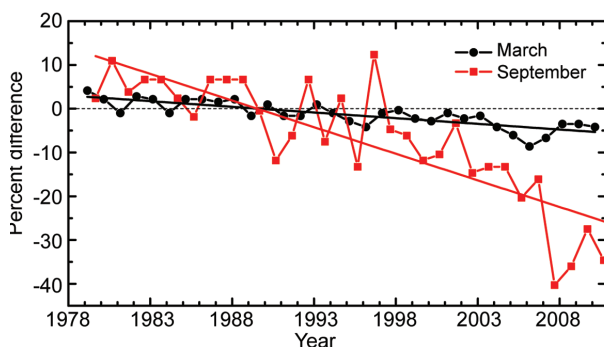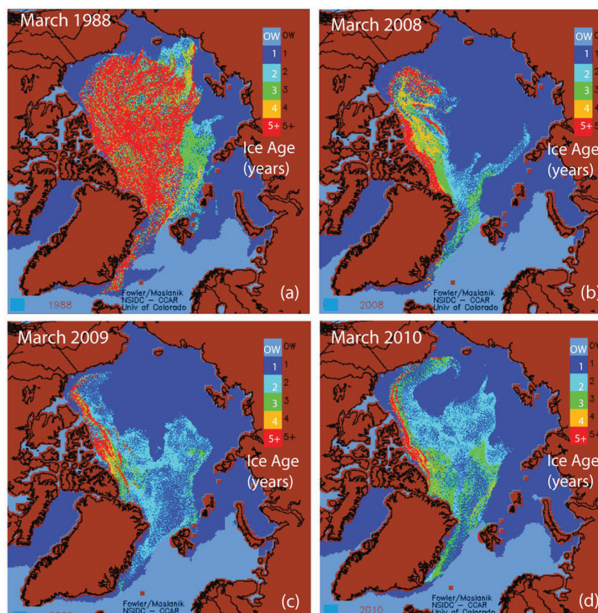

FIG. 5.11. Time series of ice extent anomalies in March (month of ice extent maximum) and September (month of ice extent minimum). The anomaly values are expressed as the percent difference between the annual value and the mean value for the period 1979–2000. The continuous straight black and red lines are regression lines that show long-term decline in the March ($R^2 = 0.66$) and September ($R^2 = 0.67$) ice extent, respectively. Based on data from National Snow and Ice Data Center, Arctic Sea Ice News and Analysis.

www.whoi.edu/beaufort) show that the pack ice in the central Canada Basin is changing from a multiyear to a seasonal ice cover.

3) Sea ice thickness

Combined estimates of ice thickness from submarine and satellite-based instruments provide the longest record of sea ice thickness observation, beginning in 1980 (Kwok et al. 2009; Rothrock et al. 2008). These data indicate that over a region covering ~38% of the Arctic Ocean there is a long-term trend of sea ice thinning over the last three decades.

Haas et al. (2010) added to this record with results from a 2009 spring field campaign of airborne electromagnetic sounding surveys of sea ice thickness at multiple locations across the Arctic Basin. Consistent with the sea ice age results presented above, the thickest ice observed was along the coast of Ellesmere Island, Canada. Mean ice thicknesses were as high as 6 m, due to extensive ice deformation along the coast. The thinnest ice was found in the Chukchi and Beaufort Seas, with average thicknesses of 1.7 m to 1.9 m. Overall, the older ice was slightly thicker in 2009 relative to 2007. The 2009 modal thickness of undeformed first year ice was unchanged from 2007.

It is instructive to examine in detail the survey site in the Lincoln Sea north of Ellesmere Island (around 62.5°W and between 83°N and 84°N), which has been part of a sea ice mass balance observation program carried out in the same region since 2004 (Haas et al. 2010). The mean ice thickness in spring 2010 was 4.02 m (± 2.10 m standard deviation), with a modal thickness (representing multiyear ice) of 3.4 m. A comparison with thickness distributions from previous years shows that ice thicknesses were very large and relatively constant from 2004 to 2006. Then, more pronounced interannual variability was observed, with minimum thicknesses in 2008 (mean 4.37 ± 1.95 m, mode 3.2 m) and a temporal recovery in 2009. The more recent variability may be related to the reduced area and decreasing age of old ice north of Ellesmere Island (Fig. 5.12).

Other airborne electromagnetic surveys were performed in April in the Beaufort and Chukchi Seas and in April and August in Fram Strait by the Alfred Wegener Institute, Germany. While there was little change since 2007 in the Beaufort and Chukchi Seas, ice thicknesses in Fram Strait were as much as 0.5 m lower than in 2009 (S. Hendricks 2010, personal communication), which is most likely related to the strong interannual and spatial variability typical for Fram Strait.

e. Land

1) Vegetation—D. A. Walker, U. S. Bhatt, T. V. Callaghan, J. C. Comiso, H. E. Epstein, B. C. Forbes, M. Gill, W. A. Gould, G. H. R. Henry, G. J. Jia, S. V. Kokelj, T. C. Lantz, S. F Oberbauer, J. E. Pinzon, M. K. Raynolds, G. R. Shaver, C. J. Tucker, C. E. Tweedie, and P. J. Webber

Circumpolar changes to tundra vegetation are monitored from space using the Normalized Difference Vegetation Index (NDVI), an index of vegetation greenness. In tundra regions, the annual maximum NDVI (MaxNDVI) is usually achieved in early August and is correlated with above-ground biomass, gross ecosystem production, CO_2 fluxes, and numerous other biophysical properties of tundra vegetation (Tucker et al. 1986; Stow et al. 2004). MaxNDVI is obtained each year from a 29-year record of NDVI derived from the AVHRR sensors on NOAA weather satellites (Bhatt et al. 2010).

MaxNDVI has increased during the period of satellite observations (1982–2010) in Eurasia and North America (Fig. 5.13a), supporting model predictions that primary production of Arctic tundra ecosystems will respond positively to increased summer warmth (Bhatt et al. 2008; Lawrence et al. 2008). Despite considerable spatial variation in the magnitude of change in each of the three variables examined, annual MaxNDVI patterns were also positively and significantly correlated with more abundant ice-free coastal waters (Fig. 5.13a) and higher tundra land temperatures (Fig. 5.13b) over most of the Arctic region (Bhatt et al. 2010). Trends in summer open water, summer land-surface temperatures, MaxNDVI, and time-integrated NDVI (TI-NDVI) in the adjacent land areas were calculated for the major sea basins in the Arctic. TI-NDVI is the sum of maximum NDVI occurring in bi-weekly intervals, and provides a perspective that includes the length of the growing season. For example, not only does Baffin Bay have a moderate MaxNDVI increase (13%) but it also has the largest TI-NDVI increase (38%). This indicates that major changes in greenness have occurred over the length of the growing season, likely due to extension of the snow-free and growing seasons (see sections 5e4 and 5f). Several new features are apparent that were not present in the *BAMS State of the Climate in 2009* (Walker et al. 2010). For example, the sea ice changes occurring in the eastern Kara Sea far exceed those elsewhere, but there has been no warming over adjacent lands or a major increase in MaxNDVI, as would have been expected. Instead, the adjacent land areas have cooled slightly and there is only a modest increase in NDVI.
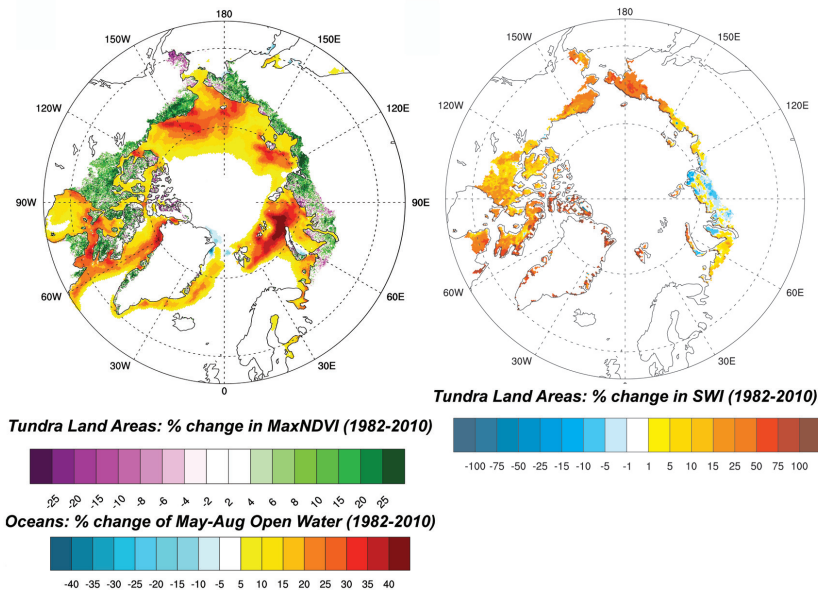
Fig. 5.13. Trends for (a) summer (May–August) open water and annual MaxNDVI, and (b) land-surface summer warmth index (annual sum of the monthly mean temperatures > 0°C) derived from AVHRR thermal channels 3 (3.5–3.9 μm), 4 (10.3–11.3 μm) and 5 (11.5–12.5 μm). Trends were calculated using a least squares fit (regression) at each pixel. The total trend magnitude (regression times 29 years) over the 1982–2010 period is expressed as a percent of the 1982 value.

Temporal changes in MaxNDVI for Arctic areas in Eurasia and North America show positive and nearly parallel increases amounting to a MaxNDVI increase of 0.02 NDVI units per decade (Fig. 5.14a). However, there is considerable variability in the rate of increase in different regions of the Arctic. For example, the MaxNDVI increase adjacent to the Beaufort Sea (+26%) is the most rapid in the Arctic and corresponds to large changes in open water (+31%) and summer land temperature (+17%). On the other hand, the MaxNDVI change in the western Kara Sea is among the smallest (+4.4%), corresponding to smaller changes in sea ice (+20%) and land temperatures (-6%; Fig. 5.14b).

In 2009 there was a circum-Arctic decrease in NDVI (Fig. 5.14a) that corresponded to elevated atmospheric aerosols over the Arctic in the same year (Stone et al. 2010). This coincided with generally lower temperatures across the Arctic in 2009 and 2010 (see section 5b). The elevated aerosols were attributed to an accumulation of pollutants in the upper troposphere from Eurasian industrial centers in combination with volcanic plumes from the eruption of Mount Re-

doubt in Alaska. The enhanced Arctic haze in 2009 was estimated to have reduced net shortwave irradiance by about 2 W m^{-2}–5 W m^{-2} (Stone et al. 2010).

Bi-weekly NDVI data reveal clear differences in phenological (green-up) patterns in North America and Eurasia (Fig. 5.15). Both regions show a ~0.06 unit MaxNDVI increase over the 29-year record. In Eurasia there is a somewhat more rapid green-up and peak NDVI was reached about 2 weeks earlier during 2000–09 than in the 1980s. In North America there is no significant shift in peak greenness. Neither continent shows a significant trend toward a longer growing season. However, whole-continent data appear to mask changes along latitudinal gradients and in different regions. For example, during 1982–2003, MaxNDVI along the Canadian Arctic climate gradient showed a ~1-week shift in the initiation of green-up and a somewhat delayed onset of senescence in the Low Arctic (Jia et al. 2009). The High Arctic did not show earlier initiation of greenness, but did show a ~1–2 week shift toward earlier MaxNDVI.

The increased Arctic greening observed in the satellite data is also observed in long-term in situ vegetation measurements. For example, the InternationTundra Experiment (ITEX), established in 1990, has made annual measurements of plant growth and
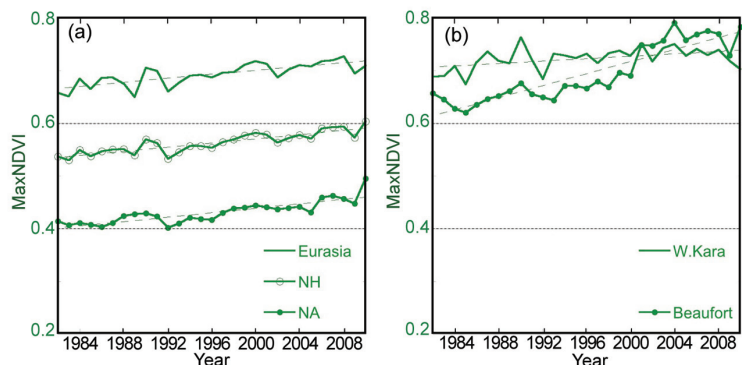

Fig. 5.14. Time series of MaxNDVI during 1982–2010 for coastal tundra in the (a) Northern Hemisphere as a whole, Eurasia, and North America, and (b) western Kara Sea and Beaufort Sea.
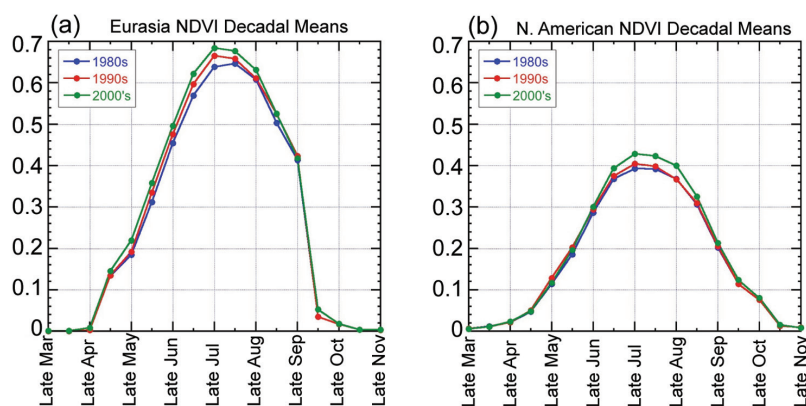
Fig. 5.15. Decadal changes in NDVI-derived phenology in (a) Eurasia and (b) North America.

phenology for up to 20 years using standardized protocols (Henry and Molau 1997). A recent synthesis of the long-term ITEX warming experiments has shown that effects on plant phenology differ by trait, community, and functional types (Elmendorf et al. 2010). Some of these results indicate there have been productivity increases consistent with warming (e.g., Hill and Henry 2011). In others, the links between local climate warming and vegetation change found in the NDVI data were not supported at the plot scale. There is a need for more careful evaluation of the causes of the observed changes, which may be driven by local long-term non-equilibrium factors other than climate warming, such as recovery from glaciation or changes in snow cover or precipitation (Troxler et al. 2010; Mercado-Díaz and Gould 2010).

The Back to the Future International Polar Year project, which revisited numerous Arctic research sites established between 15 and 60 years ago, is revealing decadal-scale changes. These include vegetation change and increases in plant cover at Barrow, Alaska, on Baffin Island, and at multiple sites throughout Beringia (Tweedie et al. 2010). Advanced phenological development and species shifts associated with drying occurred on Disko Island, Greenland. Warming of permafrost was documented in sub-Arctic Sweden, and dramatic changes in pond water column nutrients, macrophyte cover, and chironomid assemblages have been noted near Barrow. NDVI, gross ecosystem production, and methane efflux from wet vegetation types have increased at sites near Barrow, on Baffin Island and at the Stordalen mire in sub-Arctic Sweden. In most cases, air and ground warming appear to be the primary causes of change, but disturbances of various types are causing change at some sites (Johnson et al. 2010). Warming will cause changes in species distributions

and biodiversity in the Arctic. Consequently, the Circumpolar Biodiversity Monitoring Program is launching an integrated biodiversity monitoring plan for Arctic land and freshwater ecosystems (McRae et al. 2010).

Other Arctic vegetation changes indirectly related to climate include those associated with landslides, thermokarst, and fires, which are increasing in frequency in several regions (e.g., Goosef et al. 2009; Lantz et al. 2010a,b; Mack et al. 2011 in revision; Rocha and Shaver 2011). Higher soil temperatures, thawing permafrost, more abundant water, and increased nutrients due to such disturbances result in pronounced greening often due to more abundant shrub growth. Increasing air and ground temperatures are predicted to increase shrub growth in much of the Arctic, with major consequences for ecosystems (Lantz et al. 2010b). Several studies have observed increased shrub growth due to artificial warming, although the increases are small and frequently not statistically significant (e.g., Bret-Harte et al. 2002). On the other hand, there is growing evidence for increased shrub abundance at climatically- and anthropogenically-disturbed sites (Lantz et al. 2010a,b; Walker et al. 2011). In the Russian Arctic, erect deciduous shrub growth closely tracks both the recent summer warming of ~2°C over more than half a century and a trend of increasing NDVI since 1981 (Forbes et al. 2010).

2) Permafrost—V. Romanovsky, N. Oberman, D. Drozdov, G. Malkova, A. Kholodov, and S. Marchenko

Observations show a general increase in permafrost temperatures during the last several decades in Alaska (Romanovsky et al. 2007; Osterkamp 2008; Smith et al. 2010), northwest Canada (Couture et al. 2003; Smith et al. 2010), Siberia (Oberman 2008; Drozdov et al. 2008; Romanovsky et al. 2010a) and Northern Europe (Harris and Haeberli 2003; Christiansen et al. 2010).

Most of the permafrost observatories in Alaska show a substantial warming during the 1980s and especially in the 1990s. The magnitude and nature of the warming varies between locations, but is typically from 0.5°C to 2°C at the depth of zero seasonal temperature variations (Osterkamp 2008). However, during the 2000s, permafrost temperature has been

relatively stable on the North Slope of Alaska (Smith et al. 2010), and there was even a slight decrease (0.1°C–0.3°C) in the Alaskan interior during the last three years. The exception has been at Alaskan coastal sites, which have exhibited continuous warming during the last ten years. The warming trend at the Alaskan coastal sites has been particularly pronounced during the last four to five years (Fig. 5.16a). Data obtained in 2010 in Alaska suggest that the observed warming trend along the coast has begun to propagate south towards the northern foothills of the Brooks Range (approximately 200 km inland), where a noticeable warming in the upper 20 m of permafrost has become evident since 2008 (Fig. 5.16b).

A common feature at Alaskan, Canadian, and Russian sites is more significant warming in relatively cold permafrost than in warm permafrost in the same geographical area (Romanovsky et al. 2010b). Permafrost temperature has increased by 1°C to 2°C in northern Russia during the last 30 to 35 years. An especially noticeable temperature increase was observed during the last three years in the Russian Arctic, where the mean annual temperature at 15 m depth increased by > 0.35°C in the Tiksi area and by 0.3°C at 10 m depth in northern European Russia. However, relatively low air temperatures during summer 2009 and the following winter interrupted this warming trend at many locations in the Russian Arctic, especially in the western sector. Data on changes in the active layer thickness (ALT) in the arctic lowlands are less conclusive. In the Alaskan Arctic, ALT experiences a large interannual variability, with no discernible trends; this is likely due to the short length of historical data records and possible surface subsidence upon thawing of the upper, ice-rich permafrost (Streletskiy et al. 2008). At the same time, data from northern Quebec (Smith et al. 2010) and from the Nordic countries (Christiansen et al. 2010) show a distinct increasing trend in ALT during the last two decades.

The last 30 years of increasing permafrost temperatures have resulted in the thawing of permafrost in areas of discontinuous permafrost in Russia (Oberman 2008; Romanovsky et al. 2010a). This is evidenced by changes in the depth and number of taliks (a sub-surface layer of year-round unfrozen ground within permafrost), especially in sandy and sandy loam sediments compared to clay. A massive development of new closed taliks in some areas of the continuous permafrost zone, resulting from increased snow cover and warming permafrost, was responsible for the observed northward movement of the boundary between continuous and discontinuous permafrost by several tens of kilometers (Oberman and Shesler 2009; Romanovsky et al. 2010a).

3) RIVER DISCHARGE—A. I. Shiklomanov and R. B. Lammers

River discharge from Eurasia to the Arctic Ocean during 1936–2009 increased at a mean rate of 2.7 ± 0.5 km^3 yr^{-1}. For the six largest Eurasian rivers (Severnaya Dvina, Pechora, Ob, Yenisey, Lena, and Kolyma), the most significant positive trend, 12 km^3 yr^{-1}, occurred during the last 23 years (1987–2009; Shiklomanov and Lammers 2009). Data available online from the U.S. Geological Survey (http://waterdata.usgs.gov/ak/nwis) and Environment Canada (http://www.wsc.ec.gc.ca/applications/H2O/index-eng.cfm) for 2009 showed 9% higher discharge
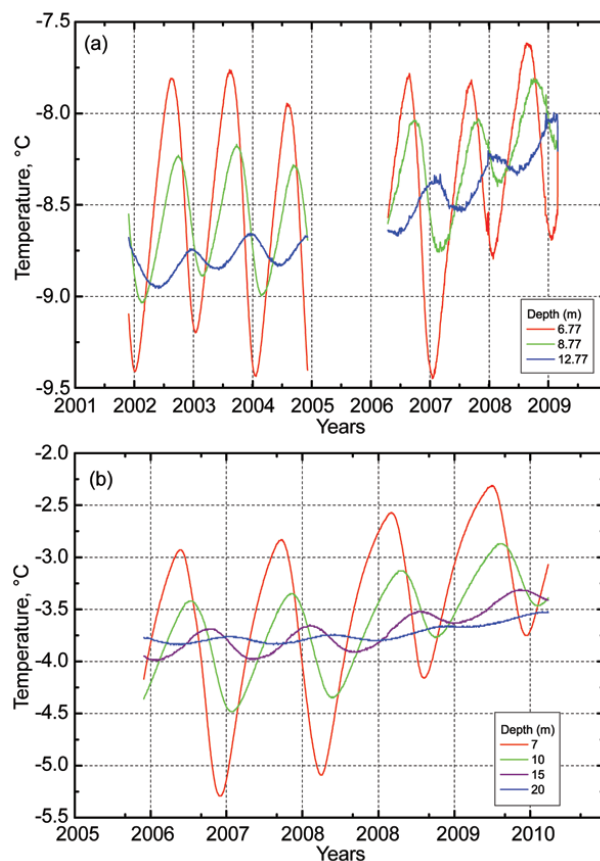
FIG. 5.16. Changes in permafrost temperature (a) between 2002 and 2009 at three different depths at the Barrow Permafrost Observatory on the northernmost coast of Alaska, and (b) between 2006 and 2010 at four different depths at the Imnaviat Creek Permafrost Observatory near the Toolik Lake research station, Alaska, approximately 200 km south of the Beaufort Sea coast. Note that the coastal permafrost (a) is colder than the inland permafrost (b). The gap in (a) between 15 May 2005 and 23 Sep 2006 is due to a datalogger malfunction.

over the 1969–2008 mean for the four largest North American rivers (Mackenzie, Yukon, Back, and Peel) flowing into the Arctic.

Officially-distributed river discharge data are usually processed and published after some delay (Shiklomanov et al. 2006). Through cooperation of the State Hydrological Institute and the Arctic and Antarctic Research Institute (AARI) in St. Petersburg, Russia, river discharge is estimated from the most important Russian monitoring sites in near real-time using provisional stage measurements, air temperature, and river ice data (http://neespi.sr.unh.edu/maps). Due to limited data availability, this technique cannot currently be applied to estimate near real-time river discharge for sites in North America.

Using this approach, the total annual discharge from the five largest Eurasian rivers (excluding the Kolyma) flowing into the Arctic Ocean in 2010 was estimated to be 1760 km^3, which is slightly higher than the long-term (1936–2009) mean of 1737 km^3. In 2010 the Yenisey discharge was 6% higher than the long-term mean and the discharge of both the Lena and Ob basins was close to the mean (Fig. 5.17, inset). During the same period, European Russia rivers (Sev. Dvina and Pechora) had 10% lower flow than the long-term mean. This was expected given the very dry and warm summer in 2010 across European Russia (see Sidebar 7.8).

An aggregated hydrograph for the five largest Eurasian rivers, based on provisional discharge estimates for 2010, is compared with discharge variability and the long-term mean hydrograph for 1994–2009, when the anthropogenic impact on discharge of these rivers was relatively stable and all variations can be attributed to the climate (Fig. 5.17). Aggregated 2010 Eurasian river discharge to the Arctic Ocean had an earlier spring snowmelt rise leading up to the peak flow and a more rapid recessional limb as the snowmelt pulse declined in the early summer. This is consistent with 2010 snow cover observations (see section 5e4) and expected changes in timing of river discharge due to increased warming in the region (Shiklomanov et al. 2007).

4) TERRESTRIAL SNOW—C. Derksen and R. Brown

In 2010, a combination of low winter snow accumulation and above-normal spring temperatures created new record-low spring snow cover duration (SCD) over the Arctic since satellite observations began in 1966. Record persistence of the negative phase of the North Atlantic Oscillation (NAO) during the winter of 2009/10 (Cattiaux et al. 2010) favored cold, dry conditions and below-average snow accumulation over large areas of Eurasia and Alaska (Fig. 5.2b). In the spring, the advection of southerly air masses was responsible for high positive air temperature anomalies over much of Eurasia and the western North American Arctic (Fig. 5.2c), which contributed to early snow melt.

Annual SCD anomalies for the 2009/10 snow year (August–July) computed from the NOAA Interactive Multisensor Snow and Ice Mapping System (IMS) 24-km product (Helfrich et al. 2007) show below-average SCD over much of the Arctic land area (Fig. 5.18a). The exception was Scandinavia which, like much of the midlatitude regions, had SCD anomalies that were largely positive. The difference in the sign of the SCD anomalies for the Arctic (positive) versus the midlatitudes (negative) reflects the Warm Arctic-Cold Continent atmospheric circulation pattern described in section 5b. Snow cover duration was computed separately for the first (August–January) and second (February–July) halves of the 2009/10 snow year using the weekly NOAA Climate Data Record (CDR; maintained at Rutgers University) to provide information on changes in the start and end dates of snow cover. While the timing of the onset of snow
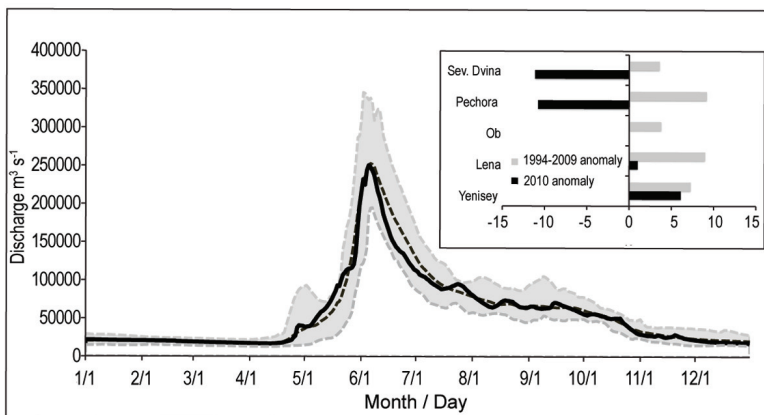
FIG. 5.17. Aggregate daily discharge hydrograph of the five largest rivers in the Eurasian Arctic in 2010 (solid black line) and long-term mean hydrograph (dashed black line) with discharge variation (gray area) during 1994–2009. Inset shows 2010 (black bars) and 1994–2009 (gray bars) anomalies relative to the long-term mean during 1936–2009 for these five rivers. Provisional estimates of annual discharge in 2010 for the five major Eurasian Arctic rivers are based on near real time data.

cover in fall continued to show little change over the satellite record (Fig. 5.18b), a new record-low spring SCD was observed over both the North American and Eurasian sectors of the Arctic during 2010 (Fig. 5.18c). This continued the trend to earlier spring snow melt over the Arctic, identified using multiple datasets (Brown et al. 2010) and reflected in the positive NDVI trends reported in section 5e1.

Northern Hemisphere spring snow cover extent (SCE), for months when snow cover is confined largely to the Arctic (Fig. 5.18d), continued to show decreasing trends that increase in magnitude over the April–June period in response to poleward amplification of SCE sensitivity to warming (Déry and Brown 2007).

Arctic snow water equivalent (SWE) time series were derived for 1990 through 2010 from two satellite passive microwave algorithms (Pulliainen 2006; Derksen et al. 2010), the Canadian Meteorological Centre (CMC) daily gridded global snow depth analysis (Brasnett 1999; Brown and Brasnett 2010), and ERA-interim atmospheric reanalysis (Simmons et al. 2007). In 2010, regionally-averaged April SWE anomalies (the month of maximum accumulation) were positive for North America, and near normal for Eurasia (Fig. 5.18e). Prior to 2004, SWE anomalies across the North American Arctic were out of phase with Eurasia, but both sectors are characterized by increasing SWE anomalies since then.

Mean monthly snow depth anomalies for April, derived from the CMC analysis, show unusually shallow snow over Alaska, sub-Arctic Canada, central Siberia, and western Russia, and deeper-than-normal snow over eastern Siberia and the eastern Canadian Arctic (Fig. 5.18f).

In summary, different regional responses to the strongly negative NAO during the snow accumulation season produced spatial variability in snow depth anomalies. A region-wide record early spring snow melt, however, resulted in a shorter-than-normal snow season across the pan-Arctic. Time series of snow parameters that extend over the past 40 years show general increases in SWE coupled with reduced spring SCD. These trends are consistent with earlier peak stream flow, a more rapid recessional limb, and higher peak runoff volumes noted in section 5e3.
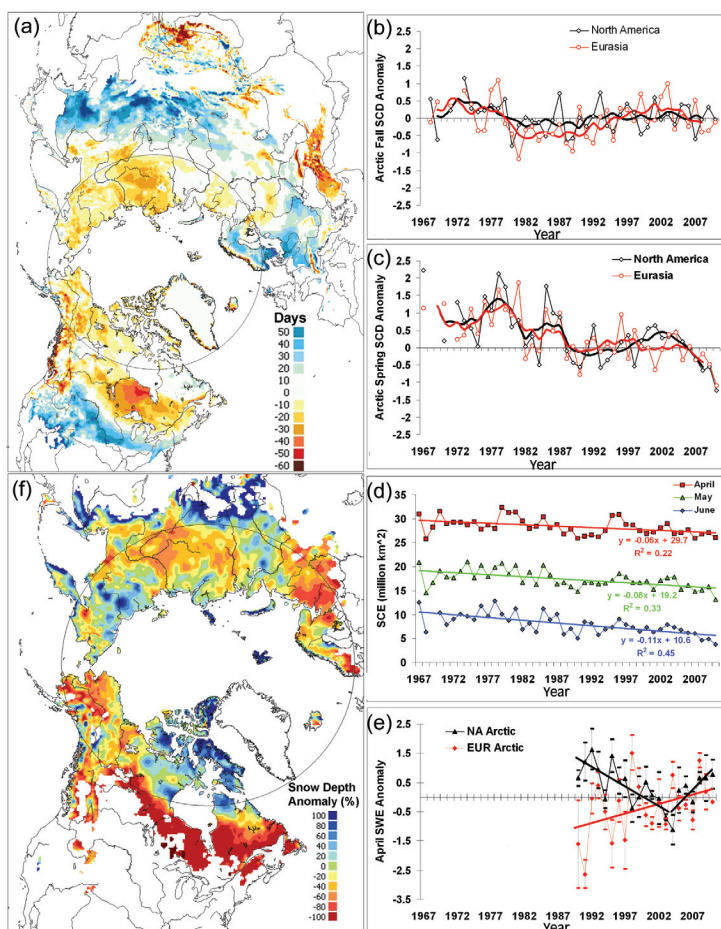

FIG. 5.18. (a) Annual snow cover duration (SCD) departures for the 2009/10 snow year (with respect to 1998–2010) from the NOAA IMS record. Arctic seasonal SCD standardized anomaly time series (with respect to 1988–2007) from the NOAA CDR record for (b) the first (fall) and (c) second (spring) halves of the snow season. Solid lines denote 5-yr moving average. (d) Monthly Northern Hemisphere snow extent from the NOAA CDR record for April, May, and June, 1967–2010. Solid lines denote linear trends (significant at 99%). (e) Multi-dataset time series of April snow water equivalent (SWE) standardized anomalies (± the standard error) relative to 1999–2009. (f) Mean monthly snow depth anomaly (% of 1999–2009 average) from the CMC snow depth analysis for April 2010.

5) GLACIERS OUTSIDE GREENLAND—M. Sharp and G. Wolken

Mountain glaciers and ice caps in the Arctic, with an area of > 400 000 km², are a significant contributor to global sea level change (Meier et al. 2007). They lose mass by surface melt and runoff and by iceberg calving. The net surface mass balance (B_n, the difference between annual

snow accumulation and annual runoff) is widely used as a measure of glacier response to climate variability and change. In cold, dry regions like the Canadian High Arctic, interannual variability in B_n is largely coupled to variability in mean summer temperature, while in more maritime regions like Iceland and southern Alaska, it is also affected by variability in winter precipitation.

As measurements for the 2009/10 balance year are not yet available, measurements are summarized here for 2008/09. These are available for twenty glaciers: three in Alaska, four in Arctic Canada, nine in Iceland, and four in Svalbard. Nineteen of the glaciers had a negative annual balance and only one (Dyngjujökull in Iceland) had a positive balance. As predicted in last year's report (Sharp and Wolken 2010), measured mass balances were more negative than in 2007/08 in Svalbard, less negative in Iceland, and very negative in Alaska where, according to GRACE satellite gravimetry, the regional net balance for all Gulf of Alaska glaciers was -151 ± 17 Gt yr^{-1}, the most negative annual value in the GRACE record (A. Arendt and S. Luthcke 2011, personal communication). In Arctic Canada, surface mass balances of three of the four glaciers measured were among the six most negative balances in the 44- to 49-year record, extending the period of very negative balances that began in 1987.

The continued breakup of the floating ice shelves that fringe northern Ellesmere Island has been associated with recent warm summers. Large new fractures were detected in the Ward Hunt Ice Shelf on 7 and 14 August 2010, and further break up of the eastern part of the ice shelf was underway on 18 August. Some 65 km^2–70 km^2 of the ice shelf was lost by the end of August (Sharp and Wolken 2010).

Data from the NCEP/NCAR R1 Reanalysis illustrate meteorological conditions over the major glaciated regions of the Arctic in the 2009/10 mass balance year (Table 5.1). Winter (September 2009–May 2010) precipitation was near normal (relative to the 1948–2008 mean) over many of the major glaciated regions of the Arctic outside Greenland, significantly above normal in Arctic Canada and Novaya Zemlya, and below normal in southern Alaska, consistent with April terrestrial snow depth anomalies (see section 5e4). Summer (June–August 2010) temperatures at 700 hPa were anomalously positive over a region including Iceland, Greenland, the Canadian Arctic, and northern Alaska, but anomalously negative over the Eurasian Arctic, especially over Novaya Zemlya (Table 5.1; see also Fig. 5.2d). This pattern is mirrored in that of 700 hPa geopotential height anomalies,

which were positive on the North American side of the Arctic and negative on the Eurasian side. Anomalous air flow associated with the positive geopotential height anomalies results in anomalous poleward-directed meridional winds over Davis Strait and Baffin Bay (see section 5b). These winds may be important in transporting heat to west Greenland and the Canadian Arctic from a region around southern Greenland, where summer sea surface temperature anomalies were +1°C to +2°C. The MODIS land surface temperature (LST) product provides a measure of the likelihood of summer melting on glaciers. In 2010, summer LST anomalies (relative to 2000–10) were positive in all glaciated regions of the Arctic, except Franz Josef Land, and very positive in the Canadian Arctic, where the average LST anomalies were +1.07°C (Table 5.1).

By comparing 2009/10 meteorological conditions with those in 2008/09, and considering 2008/09 glacier mass balances, we predict that mass balances in 2009/10 were probably more negative than in the previous year in Arctic Canada and Iceland, less negative than in 2008/09 in southern Alaska, Svalbard, and Novaya Zemlya, and similar to those of 2008/09 in Severnaya Zemlya and Franz Josef Land.

f. Greenland—J. E. Box, A. Ahlstrøm, J. Cappelen, X. Fettweis, D. Decker, T. Mote, D. van As, R. S. W. van de Wal, B. Vinther, and J. Wahr

1) Coastal Surface Air Temperatures

Record-setting high air temperatures were registered at all of the west Greenland long-term meteorological stations (Table 5.2). At Nuuk (Fig. 5.19), winter 2009/10 and spring and summer in 2010 were the warmest since 1873, when measurements began. At Prins Christian Sund, as at Nuuk, 2010 annual anomalies were three standard deviations above the 1971–2000 baseline. Warm anomalies were greatest at Aasiaat, where winter temperatures were 7°C above the 1971–2000 baseline, which is three standard deviations above the mean. Temperature anomalies extended west into Arctic Canada (see also section 5e5), but not into east and northeast Greenland.

These measurements are consistent with anecdotal data provided by a long-time resident of Greenland (2010, personal communication), who wrote on 4 February 2010: "we don't have snow, we don't have the cold" ... "This weather this year is really different, in 30 years that I live in Ilulissat, that is the first year in this conditions. We have lot of dog sledding tourists, but we cannot do the tour, too much ice on the hills and dangerous to drive by sled." ... "no snow at all".

Table 5.1: Summer (June –August) 2010 700 hPa air temperature, winter (September 2009– May 2010) precipitation, and summer MODIS Land Surface Temperature (LST) anomalies for major glaciated regions of the Arctic (excluding Greenland). For ranks, 1 = year with highest summer air or land surface temperature and winter precipitation, and n is the number of years in the record. Air temperature and precipitation anomalies are relative to 1948–2008 climatology from the NCEP/NCAR R1 Reanalysis. Mean summer LST values are calculated from eight day averages of daytime, clear sky values for a period centered on 15 July of each year. The length of the measurement period varies between regions and is equal to the mean (+4 standard deviations) annual melt duration in each region during the period 2000–09 derived using microwave backscatter measurements from the Seawinds scatterometer on QuikScat. LST is measured for blocks of 1-km by 1-km cells containing only glacier ice centered on high elevation regions of major ice caps in each region. Block size varies with the size of the ice cap, but is consistent between years. LST anomalies are relative to the mean LST for the period 2000–10.

Region	Sub-Region	Latitude (°N)	Longitude (°E)	2010 Jun–Aug 700hPa T Anomaly	2010 Rank	2009–10 Sep–May Ppt Anomaly	2009–10 Rank	2010 MODIS LST Anomaly	2010 Rank
				(°C)	(n=63)	(mm)	(n=62)	(°C)	(n-11)
Arctic Canda	N. Ellesmere Island	80.6–83.1	267.7–294.1	2.68	2	28.3	4	0.56	6
	Axel Heiberg Island	78.4–80.6	265.5–271.5	1.99	4	22.5	8	1.17	3
	Agassiz Ice Cap	79.2–81.1	278.9–290.4	2.03	4	55.8	9	1.34	2
	Prince of Wales Icefield	77.3–79.1	278–284.9	2.10	3	24.5	9	1.16	2
	Sydkap	76.5–77.1	270.7–275.8	2.11	1	57.3	8	1.28	2
	Manson Icefield	76.2–77.2	278.7–282.1	2.08	2	148.9	1	1.22	1
	Devon Ice Cap	74.5–75.8	273.4–280.3	1.96	2	19.9	16	1.02	1
	North Baffin	68–74	278–295	1.67	5	52.5	7	0.89	1
	South Baffin	65–68	290 – 300	1.65	5	-24.3	42	1.00	1
Eurasian Arctic	Severnaya Zemlya	76.25–81.25	88.75 – 111.25	-0.05	29	2.7	29	0.89	1
	Novaya Zemlya	68.75–78.75	48.75 – 71.25	-0.94-9	52	86.2	5	0.44	3
	Franz Jo-sef Land	80–83	45 – 65	-0.01	32	-17	37	-0.06	7
	Svalbard	76.25–81.25	8.75 – 31.25	-0.30	44	16.9	23	0.49	2
	Iceland	63–66	338 – 346	1.62	2	-10	35	0.34	2
Alaska	SW Alaska	60–65	210 – 220	0.69	14	-29	36	0.38	3
	SE Alaska	55–60	220 – 230	0.57	17	-26	35	*0.53	2*

Later, the same source spoke of "10–12 days of" continuous "heat wave" like weather, in June, with "a lot of blue skies". Ilulissat is at 69.0°N on the west coast of Greenland, ~100 km northeast of Aasiaat, and ~560 km north of Nuuk (see Fig. 5.19).

2) Upper Air Temperatures

Seasonally-averaged 2010 upper air temperature data, available from twice-daily radiosonde observations (Durre et al. 2006), indicate a pattern of record-setting warm anomalies below 300 hPa (e.g., Fig. 5.19, inset). This is consistent with a warming trend prevailing since reliable records began in 1964 and especially since the mid-1980s (Box and Cohen 2006). Upper air temperature anomalies in 2010 are consistent among all stations, but, as at the surface stations, they are most pronounced in central-west Greenland (Table 5.2) and closest to normal in east Greenland.
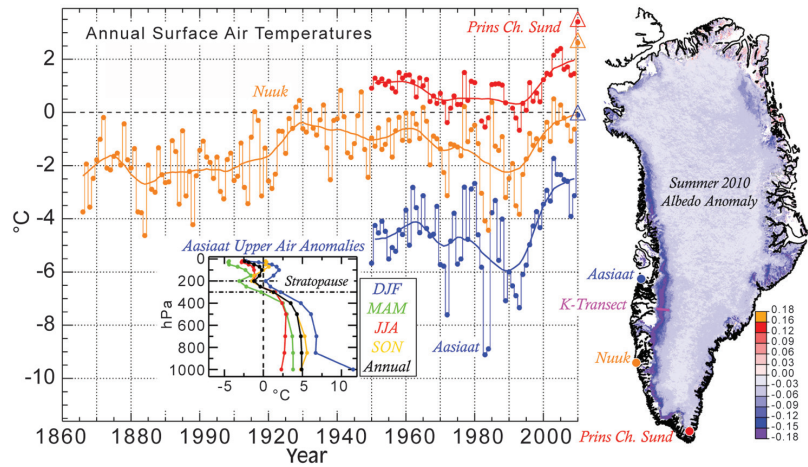

FIG. 5.19. Three Greenland meteorological station records illustrating the long-term time series of yearly-average temperatures. Triangles denote record-setting values, all in 2010. The inset shows upper air temperature anomalies in 2010 at Aasiaat relative to the 1971–2000 baseline. The map on the right shows summer (June–August) Greenland ice sheet surface albedo changes (from **MODIS MOD10A1 data**) and locations of meteorological stations and the K-Transect.

3) Atmospheric Circulation

The high, positive temperature anomalies over the inland ice sheet are largely explained by atmospheric circulation anomalies. NCEP/NCAR Reanalysis data

Station (Region), Latitude, Longitude, time range	Winter	Spring	Summer	Autumn	Annual
Table 5.2. 2009 Greenland station surface air temperature anomalies by season, relative to 1971–2000.					
Thule AFB/Pituffik (NNW), 76.5° N. 68.8°W, 1961–2010	**4.1**	**2.6***	**1.3**	2.4	**2.1***
Upernavik (NW), 72.8°N, 56.2°W, 1873–2010	**6.1**	**4.0**	**1.4**	**2.8***	**3.7***
Aasiaat (W), 68.7°N, 52.8°W, 1951–2010	**7.1***	**5.2***	**1.5**	**2.5***	**4.1***
Nuuk (SW), 64.2°N, 43.2°W, 1873–2010	**5.4***	**3.6**	**2.1***	**3.3***	**3.8***
Prins Christian Sund (S), 60.0°N, 43.2°W, 1951–2010	**3.1***	1.5	**1.8***	**2.0***	**2.3***
Tasiilaq (SE), 65.6°N, 22.0°W, 1895–2010	**3.1**	0.8	**1.8**	1.0	**1.8**
Illoqqortoormiut (E), 70.4°N, 22.0°W, 1948–2010	0.3	-0.8	0.0	0.2	-0.1
Danmarkshavn (NE), 76.8°N, 18.8°W, 1949–2010	0.7	0.6	0.1	-0.4	0.0

*Bold values indicate anomalies that meet or exceed one standard deviation from the mean. Underlined values exceed two standard deviations from the mean. Italicized values exceed three standard deviations from the mean. Asterisks indicate record-setting anomalies. Winter values include December of the previous year.

for 2010 indicate abnormally large heat flux from the south over the southwestern part of the Greenland ice sheet. NCEP/NCAR Reanalysis geopotential height anomalies at 500 hPa in June, July, and August 2010 (referenced to the 1971–2000 baseline) were at least twice the 1971–2000 standard deviation (see also section 5b.).

4) Surface Melt extent and Duration and Albedo

The areal extent and duration of melting on the ice sheet, derived from daily passive microwave satellite remote sensing observations (Mote 2007), continued to increase in 2010. During April–September 2010 the melt area was ~8% more extensive than the previous record set in 2007 (Fig. 5.20). The 2010 melt extent through mid-September was 38% greater than the 1979–2007 average, and the June–August extent was 26% greater than the 1979–2007 average. Compared to summer 2007, when melt anomalies occurred in both the ablation and percolation zones (Tedesco et al. 2008), 2010 melt anomalies were concentrated in the lower elevation bare ice zone.

Abnormal melt duration was concentrated along the western margin of the ice sheet. This was consistent with the anomalous summer heat flux described above, preceded by abnormally high winter air temperatures that led to warm conditions prior to the onset of melt (Tedesco et al. 2011). The melt duration was as much as 50 days greater than average at elevations between 1200 and 2400 meters above sea level in west Greenland. In May, low elevation areas along the western ice margin melted for as much as 15 days longer than average.

The melt extent and duration observations are consistent with the observed coastal and upper air temperatures described above, and derived meteorological data. For example, NCEP/NCAR Reanalysis data suggest that May surface temperatures were up to 5°C above the 1971–2000 average. In June and August there were large positive degree day anomalies (up to 20 degree days) along the western and southern ice sheet. During August, temperatures were 3°C above average over most of the ice sheet, with the exception of the northeastern region. In August along the southwestern inland ice sheet, there has been an increase of 24 melting days during the past 30 years of passive microwave data coverage.

As melt extent and duration have increased during the last decade, MODIS10A1 data (Hall et al. 2006) indicate that the surface albedo of the ice sheet has also decreased, particularly along the western margin of the sheet (Fig. 5.19). The albedo decrease has been concentrated where bare ice has been exposed once the snow from the previous winter has melted away by mid-summer peak solar irradiance.

5) Surface Mass Balance along the K-Transect

The 150-km long K-Transect is located near Kangerlussuaq at 67°N between 340 m and 1500 m above sea level on the western flank of the ice sheet (van de Wal et al. 2005; Fig. 5.19). The surface mass balance between September 2009 and September 2010 was by far the lowest since 1990, when routine measurement began. Averaged over the length of the transect, the surface mass balance was 2.7 standard deviations below the 1990–2010 average. The altitude of the snow line, which describes the maximum areal extent of melting of the snow cover since the previous winter, was the highest on record, and a melt season that began very early (late April) continued until the beginning of September. Surface albedo values at the weather stations were below average and summer air temperatures were above average. In south Greenland, where the highest net ablation (~6 m of ice) of Greenland is found at low elevation, 2010 was unique in the observations since 1991, with about 9 m of ablation due to early melt and the lack of the commonly abundant winter precipitation, which usually takes one to two months to melt away.

The apparently strong link between negative surface mass balance and observed high air temperatures due to strong heat flux from the south and the record-high melt extent and duration, has been successfully simulated by the Modèl Atmosphérique Régional (MAR) regional climate data assimilation model. It simulated an ice sheet surface mass balance 90% less positive than normal, the lowest net mass accumulation rate since 1958 when
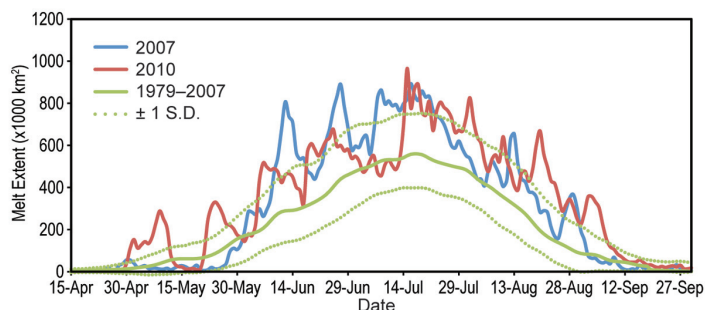

Fig. 5.20. Time series of Greenland melt extent derived from passive microwave remote sensing. The broken green lines are ±1 standard deviation (S.D) of the 1979–2007 average. After Mote (2007).

data to drive the model became available (Tedesco et al. 2011). This condition reflects a very heavy melt year combined with below-normal ice sheet snow accumulation.

6) Total Greenland Mass Loss from GRACE

GRACE satellite gravity solutions (Velicogna and Wahr 2006) are used to estimate monthly changes in the total mass of the Greenland ice sheet. For the hydrologic year 2009/10, i.e., from the end of the 2009 melt season, including October, through the end of October 2010, the ice sheet cumulative loss was -410 Gt, 177% (or two standard deviations) of the 2002–09 average annual loss rate of -231 Gt yr^{-1}. The 2010 mass loss is equivalent to a eustatic sea level rise contribution of 1.1 mm. This was the largest annual loss rate for Greenland in the GRACE record, 179 Gt more negative than the 2003–09 average. The 2009/10 hydrological year ended 206 Gt more negative than the recent (2002–09) hydrological year average. Using GRACE data, Rignot et al. (2011) found an acceleration of Greenland ice sheet mass budget deficit during 1979–2010, in close agreement with an independent mass balance model.

7) Marine-Terminating Glacier Area Changes

Marine-terminating glaciers are of particular interest because they represent the outlets through which inland ice can move most quickly and in the largest quantities out to sea. Iceberg calving from these glaciers represents an area reduction and mass loss from the ice sheet, which contributes to sea level rise.

Daily surveys using cloud-free MODIS visible imagery (Box and Decker 2011; http://bprc.osu.edu/MODIS/) indicate that, during 2010, marine-terminating glaciers collectively lost a net area of 419 km^2. This is more than three times the annual loss rate (121 km^2 yr^{-1}) of the previous eight years, 2002–09 (Fig. 5.21). The calving of 290 km^2 of ice from Petermann Glacier ice shelf in far northwest Greenland accounted for 70% of the loss (see http://bprc.osu.edu/MODIS/?p=69). Glacier ice area loss elsewhere in 2010 (i.e., excluding Petermann Glacier) remained near the average loss rate of 121 km^2 yr^{-1} observed since 2002. Glacier area change surveys (Howat and Eddy 2011) indicate that the ice area loss rate of the past decade is greater than loss rates since at least the 1980s.

A number of other large marine-terminating glaciers also lost a significant area of ice in 2010: Zachariae Isstrøm, northeast Greenland, 43 km^2; Humboldt Glacier, northwest Greenland, 20 km^2; Ikertivaq Glacier, Southeast Greenland, 15 km^2; and five glaciers that flow into Upernavik glacier bay in northwest Greenland, 14 km^2.

Since 2000, the net area change of the 39 widest marine-terminating glaciers is -1535 km^2 (17.5 times the size of the 87.5 km^2 Manhattan Island, New York) and the average effective glacier length change was -1.7 km. While the overall area change was negative, 7 of the 39 glaciers did advance in 2010 relative to 2009. The largest glacier area increases were at Ryder and Storstrømmen glaciers, 4.6 km^2 and 4.2 km^2, respectively.
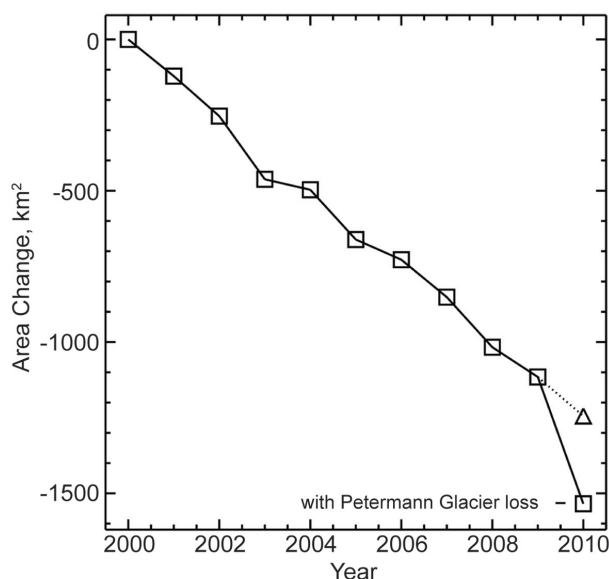

Fig. 5.21. Cumulative net annual area changes for the 35 widest marine-terminating glaciers of the Greenland ice sheet. Net area change in 2010 is shown with and without the Petermann Glacier loss. The trend without the Petermann Glacier loss in 2010 is illustrated by the triangle and dashed line.